CHAPTER 2

LITERATURE REVIEWS

This chapter introduces basic principles of thermoelectric phenomena and various thermoelectric materials used at both macro and micro scales. This chapter presents an overview of thermoelectric properties, deposition techniques and their effect on TE material quality and performance. Furthermore, it summarizes properties of several important state-of-the-art thermoelectric materials.

มหาวิทยาลัยราชภัฏสกลนคร

PRINCIPLES OF THERMOELECTRICS

Seebeck, Peltier and Thomson effects

Seebeck effect: In 1821 Thomas Johann Seebeck, first discovered the Seebeck effect. Seebeck observed detected that a compass needle deflected when placed in the vicinity of a closed loop formed of two dissimilar metals with a temperature difference between the junctions. This observation provides direct evidence that a current flow through the closed circuit is driven by the temperature difference. A temperature difference causes charge carriers (electrons or holes) in the material to diffuse from the hot side, to the cold side. Mobile charge carriers migrate to the cold side, and leave behind their oppositely charged and immobile nuclei at the hot side thus giving rise to a thermoelectric voltage. The buildup of charge carriers on the cold side eventually ceases when an equal amount of charge carriers drift back to the hot side as a result of the electric field created by the charge separation. At this point, the material reaches steady state. Only an increase in the temperature difference can resume a buildup of more charge carriers on the cold side and thus lead to an increase in the thermoelectric voltage. The thermoelectric voltage, called the thermoelectric electromotive force *(emf)*, is generated by a temperature difference between two

different materials (A and B) such as metals or semiconductors as shown in Equation (1)

$$\Delta V = (S_A - S_B)\Delta T \tag{1}$$

where, S_A and S_B are the Seebeck coefficients of materials A and B, respectively. This drives a continuous current flowing through the conductors if their junctions are kept at different temperatures. In case of an open circuit as shown in Figure 1, the charge gradient due to the diffusion current will result in the buildup of an electric field, until drift current in the opposite direction is equal to the diffusion current. The Seebeck coefficient of a material defines the strength of the electric field generated by a given temperature gradient in the material.

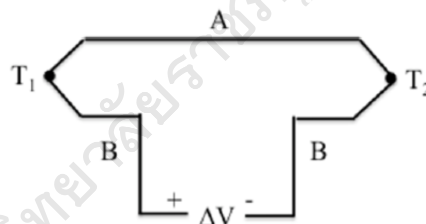

Figure 1 Seebeck effect: A temperature difference create a potential difference for the junction between materials A and B. (Ghafouri, 2012).

มหาวิทยาลัยราชภัฏสกลนคร

Peltier Effect: Heat that is generated as a result of a current flowing through a junction between two conductors. This effect was first observed in 1834 by Jean Peltier. The Peltier effect is the underlying foundation for thermoelectric refrigeration and can be regarded as the reverse of the Seebeck effect. When an electric current passes through two dissimilar materials such as metals or semiconductors that are connected at two junctions, heat will be absorbed at one junction and released at the other junction. As a result, one

junction cools off while the other heats up, depending on the direction of the current. The Peltier coefficients represent how much heat is carried per unit charge through a given material. The Peltier heat (*Q*) absorbed by the cold junction per unit time is given by:

$$\frac{dQ}{dt} = (\Pi_A - \Pi_B)I \tag{2}$$

In this equation, Π_A and Π_B are the Peltier coefficients of materials A and B.

Thomson Effect: The Thomson effect was predicted and subsequently experimentally observed by William Thomson (Lord Kelvin) in 1851. It refers to the emission or absorption of heat by a current carrying conductor exposed to a temperature gradient. If a current density J passes through a homogeneous conductor, heat production per unit volume q is :

$$q = \rho J^2 - \mu J \frac{dT}{dx} \tag{3}$$

In this equation, ρ is the electrical resistivity of the material, $\frac{dT}{dx}$ is the temperature gradient along the conductor, and μ is the Thomson coefficient. The first term in Equation (3), ρJ^2, represents the Joule heat per unit volume, which is irreversible reversible. The second term, $\frac{dT}{dx}$, is the Thomson heat, whose sign alternates when current flux, J, changes direction. The Thomson coefficient, μ, is related to the Seebeck coefficient by the following equation:

$$\mu = T \frac{dS_s}{dT} \tag{4}$$

Thermoelectric Figure of Merit

The key parameters that determine the capacity of a thermoelectric material for cooling or power generation are the Seebeck coefficient, thermal

conductivity, and electrical resistivity. The Peltier coefficient is equivalent to the Seebeck coefficient scaled by temperature. Similarly, the Thomson coefficient can be derived from the Seebeck coefficient if its value is known over of a range of temperatures. In the early 1900s, E. Altenkirch introduced the concept of thermoelectric figure of merit. It revealed that good thermoelectric materials should have low electrical resistivity to minimize heating, low thermal conductivity to maintain a large temperature gradient, and high Seebeck coefficients for maximum conversion of heat to electrical power or electrical power to cooling performance. The relationship between these properties can be quantitatively expressed by the thermoelectric figure of merit, Z, defined as :

$$Z = \frac{S_s^2}{\rho \kappa} \tag{5}$$

มหาวิทยาลัยราชภัฏสกลนคร

Since Z has a unit of K^{-1}, the dimensionless figure of merit ZT is often used as the measure of a material’s thermoelectric performance. The optimization of ZT is not simply possible by optimizing the relevant individual material properties, i.e. Seebeck coefficient, electrical and thermal conductivities. These material properties are inter-related, so optimizing one can have a negative effect on the others. In particular, carrier thermal conductivity and electrical resistivity are related through carrier concentration as well as carrier mobility and at a given temperature have a constant ratio based on the Wiedemann–Franz law.

$$\frac{\kappa}{\sigma} = LT \tag{6}$$

$$L = \frac{\pi^2}{3}\left(\frac{\kappa_B}{e}\right)^2 = 2.45 \times 10^{-8} \frac{\mathrm{W\,\Omega}}{\mathrm{K}^2}$$

where, κ_B is the Boltzmann constant and e is the electron charge Theoretical and experimental studies of solid-state materials have indicated that some

semiconductors have relatively high power factor $\frac{S^2}{\rho}$ and low thermal conductivity, which makes them a perfect fit for use in high ZT materials. However, semiconductors are not immune to the relations between various thermoelectric material properties. Both the Seebeck coefficient and resistivity are related to the separation between the conduction band in *n*-type (valence band in *p*-type) and the Fermi level of the material. As a result, attempts to raise the Seebeck coefficient by manipulating the Fermi level usually result in increase in resistivity as well. On the other hand, doping the material to increase electrical conductivity decreases the Seebeck because the Fermi level is moved close to the corresponding band edge or even into the band itself. Therefore, it is critical to find a doping level where the power factor is optimized. In order to reduce thermal conductivity, the common approach is to introduce additional short-range disorder into the crystalline structure. On the other hand, the distortion inevitably blocks charge transport, which may reduce electrical conductivity.

Seebeck Coefficient

The Seebeck coefficient of a material is a measure of the induced thermoelectric voltage produced by a temperature difference across its ends. The Seebeck coefficient is given by:

$$S_s = \frac{8\pi^2 k_B^2}{3eh^2} m^* T \left(\frac{\pi}{3n}\right)^{\frac{2}{3}} \quad (7)$$

where, k_B is the Boltzmann constant, e is the electron charge, h is the Planck constant, m^* is the effective mass, T is the temperature, and n is the carrier concentration. Based on this equation, the Seebeck coefficient is negative if carriers are electrons, positive if they are holes, and its maximum is achieved for large effective mass and low carrier concentration. In semiconductors, which are known to have high Seebeck coefficients, this relation can be defined based on the band model:

$$S_s = -\frac{k_B}{e}\left[\left(\frac{5}{2}+s\right)+\ln\frac{2\left(2\pi m^* k_B T\right)^{\frac{3}{2}}}{h^3 n}\right] \tag{8}$$

Here, S is the scattering parameter, assuming that the carrier relaxation time can be expressed in terms of carrier energy in a simple way ($\tau = \tau_0 E^s$, where τ is the carrier relaxation time, E is the carrier energy and τ_0 is a constant). It can be seen that the Seebeck coefficient is inversely related to the carrier concentration in a semiconductor. Equation 8 is for *n*-type semiconductors with electron carriers, but the same relation applies to *p*-type TE semiconductors as well.

Electrical Resistivity

The other factor that influences the TE material figure-of-merit is electrical resistivity (ρ). The material resistivity, which is expressed in Ω m, is given by:

$$\rho = \frac{1}{\sigma} = \frac{1}{en\mu} \tag{9}$$

Electrical resistivity of a material is also inversely proportional to its carrier concentration. The TE material figure-of-merit is proportional to the power factor ($\frac{S_s^2}{\rho}$). As shown in Figure 2, the power factor is related to carrier concentration and is maximized at $n \sim 10^{20}$ cm^{-3} in semiconductors.

มหาวิทยาลัยราชภัฏสกลนคร

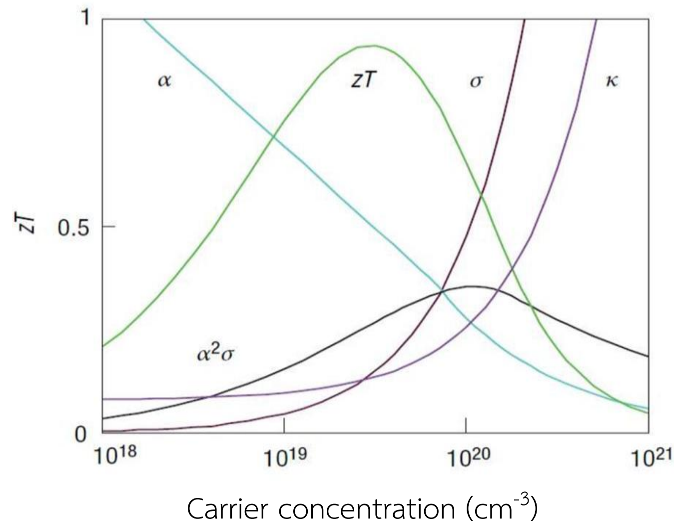

Figure 2 Effect of carrier concentration on thermoelectric properties of a material. (Ghafouri, 2012).

มหาวิทยาลัยราชภัฏสกลนคร

Thermal Conductivity

Thermal conductivity is the ability of a material to transfer heat as a result of a temperature gradient across different points. The thermal conductivity of thermoelectric materials consists of the conductance via electrons (κ_{electron}) and phonons (κ_{phonon}). Thermal conductivity through phonons is defined as follows:

$$\kappa_{\text{phonon}} = \frac{Cvl}{3} \tag{10}$$

where C is the phonon heat capacity per unit volume, v is the average phonon velocity, and l is the phonon mean free path between Umklapp scattering events. The mean free path is inversely proportional to the number of excited phonons. Therefore, phonon thermal conductivity increases as temperature decreases. This trend changes at very low temperatures where C becomes proportional to T^3, with κ_{phonon} approaching zero as the temperature approaches 0 K.

Thermal conductivity through electrons is governed by a similar equation with electron heat capacity, electron velocity and electron mean free path, and leads to the following equation:

$$\kappa_{\text{electron}} = \frac{\pi^2 n k_B^2 T \tau}{m} = \frac{\pi^2 n k_B^2 T \mu}{e} \qquad (11)$$

THERMOELECTRIC APPLICATIONS

The relation between the figure of merit and efficiency (in the case of thermoelectric power generation) or performance coefficient (in the case of thermoelectric cooling) was derived by Ioffe theoretically , after neglecting thermal and electrical contact resistances. Therefore, improving the figure of merit as the governing factor in thermoelectric materials' efficiency is the main goal of efforts to find materials for future generation thermoelectric applications.

Thermoelectric Power Generation

Thermoelectric generators convert heat into electrical power based on the Seebeck effect. The basic is illustrated in Figure 3. The thermocouples in a thermoelectric device are connected thermally in parallel and electrically in series. Heat is pumped into one side of the couple, flows through the thermocouples and rejected from the opposite side. The generator open-circuit voltage is proportional to the number of thermocouples, the Seebeck coefficients of *n*-type and *p*-type legs (S_n and S_p), and the temperature gradient between the hot and cold junctions (ΔT).

$$V = N(S_p - S_n)\Delta T \qquad (12)$$

When the generator is connected to an electrical load of resistance R_L , the Seebeck voltage produces an electrical current. The output power of the generator is given by:

$$P = \frac{V^2}{R_L} = \frac{N^2 (S_p - S_n)^2 \Delta T^2}{R_L} \quad (13)$$

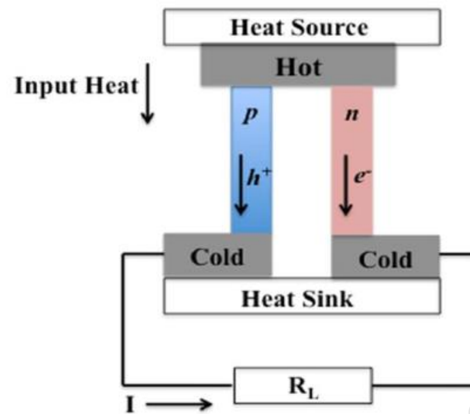

Figure 3 Illustration of thermoelectric power generation. (Ghafouri, 2012).

มหาวิทยาลัยราชภัฏสกลนคร

MAGNETRON SPUTTERING METHOD

Magnetron sputtering is a widely used technique in phase-change memory device fabrication, not only to deposit the phase-change films but also the dielectric capping layers, metallic reflective layers, etc. DC magnetron sputtering technique is employed depending on the material type. Typically, metallic or semi-metallic materials layers are coated using DC magnetron sputtering. The basic concepts of sputtering, and DC magnetron sputtering are briefly explained below.

Sputtering

Sputtering is a physical process involving removal of fractions of a material called sputtering target, and subsequent deposition onto a substrate. Sputtering is achieved by bombarding the target surface with ions under high voltage acceleration. As a result of the ion impingement, atoms (or occasionally molecules) are ejected from the target surface due to the momentum transfer by the impinging ions. Sputtering takes place usually at low pressures, typically in a range between 10^{-4} and 10^{-2} mbar. The bombard ions are formed by a glow

discharge process, where inert gas atoms are ionized by an electric discharge to form plasma. Plasma can be defined as a gas with charged and neutral particles, for example, electrons, positive ions, atoms and molecules. Overall the plasma is charge neutral. Plasma is usually created with argon gas which is fed into the sputtering chamber. Due to the natural cosmic radiation, there are always some ionized Ar^+ ions present in the chamber to the ignite plasma.

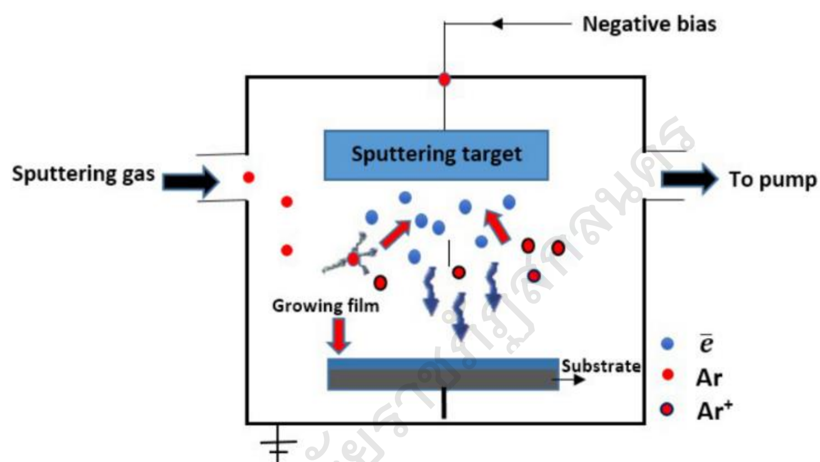

Figure 4 Schematic of a simple sputtering setup with Ar as sputtering gas.

In DC sputtering, the target is negatively biased (typically up to few hundred volts) to attract Ar^+ ions from the plasma and make collisions on the target surface. These attracted Ar^+ ions also responsible for the production of secondary electrons which cause further ionization of the sputtering gas. A sufficient ionization rate is required to sustain a stable plasma. One of the ways to increase the ionization probability is increasing the partial pressure of the sputtering gas (i.e., increasing the gas pressure, more collisions result in the formation of more ions). Increased ion current to the target results in higher depositions rate. However, at very high pressures, sputtered target atoms get scattered before reaching the target. This reduces the deposition rate. Therefore, a peak in the deposition rate versus pressure curve occurs (and for Ar ions this is

around 110 mTorr). A schematic representation of a DC sputtering setup with Ar sputtering gas is shown in Figure 4.

Magnetron sputtering

In order to get a reasonable deposition rate, a sputtering chamber must operate at relatively high pressures, which means that there is a fairly high concentration of impurities in the gas. Also, at high pressures there is a lot of interaction between gas molecules and chamber walls resulting in increased contamination from the walls. An effective solution to minimize these problems is using a magnetron. In magnetron sputtering, the use of a magnetic field to trap electrons around the target gives a higher deposition rate at lower pressures. The fraction of ions in plasma is significantly less than the total concentration of gas atoms (typical ion densities in plasma are about 0.0001%). In general, this leads to reduced deposition rates of sputtering as compared with evaporation. Magnetrons make use of the fact that a magnetic field configured parallel to the target surface can constrain the motion of secondary electrons, ejected by the bombarding ions, closely to the target surface. An array of permanent magnets is placed behind the sputtering source. The magnets are placed in such a way that one pole is positioned at the central axis of the target, and the second pole is placed in a ring around the outer edge of the target. A schematic of the magnetron assembly is shown in Figure 5.

This configuration creates crossed electric ($\boldsymbol{E}$) and magnetic (B) fields, where electrons drift with velocities (u) perpendicular to both E and B according to $u = ExB/B.B$. If the magnets are arranged in such a way that they create closed drift region, electrons are trapped, and rely on collisions to escape. By trapping the electrons in this way, the probability for ionization is increased by orders of magnitudes. Ions are also subjected to the same force, but due to their larger mass, the Larmor radius often exceeds the dimensions of the plasma chamber. The trapping of electrons creates a dense plasma, which in turn leads to an increased ion bombardment of the target, giving higher sputtering rates and, therefore, higher deposition rates at the substrate. The electron confinement also allows for a magnetron to be operated at much lower voltages compared to

basic sputtering (about 500 V instead of 2 to 3 k V) and be used at lower pressures (typically in mbar region).

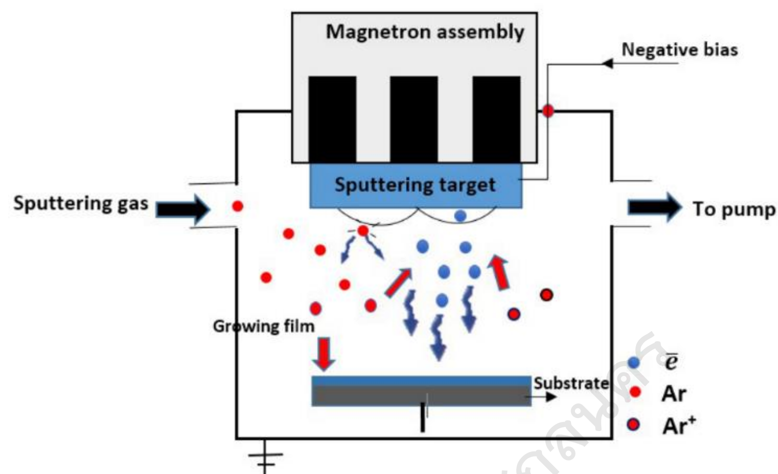

Figure 5 Schematic of a DC magnetron sputtering setup.

Features of sputtering

Sputtering has become one of the powerful techniques in modern manufacturing. In fact, today's technologists use sputtering to coat more surfaces in more industries than ever before. From semiconductors to credit cards; from compact discs to auto parts; magnetron sputtering is adding new value to a growing list of products every day. Specifically, in optical data storage applications, sputtering virtually deposits the whole variety of layers (made up of alloys, metals and compounds) used in the optical disk formats and provides a unique combination of advantages. The specific advantages of sputtering are :

1) A high kinetic energy of sputtered atoms providing better film adhesion.

2) Since coverage is independent of line of sight, sputtering inherently produces uniform film coatings over a large area.

3) Unlike evaporation techniques, which require horizontal placement of the crucible containing molten material and vertical placement below the substrate, sputtering works in any orientation, provided it faces the substrate.

4) It offers much greater versatility than other approaches because, as a cold momentum transfer process, it can be used to apply either conductive or insulating materials to any type of substrate including heat sensitive plastics, e.g. polycarbonate typically used in optical disks.

5) Sputter cleaning of the substrate in vacuum prior to film deposition can be done.

6) It enables simultaneous deposition from multiple sources to develop new alloys.

7) For industrial applications (i.e. for the bulk production of devices), sputtering can be made a continuous, inline process. Deposition of multiple layer stacks is possible (for e.g. to deposit various layers of an optical disk) by having multiple chambers, in a row, with sputter cathodes of different materials.

8) Tuning of specific film properties (for e.g. composition, microstructure, step coverage) can be more easily achieved, than any other techniques, by varying the sputtering parameters (single or multiple parameters) such as target to substrate spacing, sputtering gas pressure, sputtering gas/ion type, biasing the substrate.

9) Compound thin films can be deposited using reactive sputtering i.e. sputtering in the presence of a reactive gas. Typically oxides or nitrides of phase-change materials are deposited by this method.

THERMOELECTRIC PROPERTIES MEASUREMENT AND DETERMINATION

Electrical properties of film

The electrical properties include electrical resistivity, mobility and carrier concentration, which is available from Hall effect.

1. Electrical resistivity

Electric current has the solid conductor which potential difference, Typically, the current density (J) proportional to the electric field (E) ;

$$J = \frac{E}{\rho} = \sigma E \tag{14}$$

where, ρ is electrical resistivity (Ω m) and σ is electrical conductivity (S cm^{-1}), equation (14) shows Ohm's Law in figure 2.7 shows that the measurement of electrical resistivity while a current flows through a conductor with a cross section constant and the electric potential difference $(V_2 - V_1)$ measurement between two points.

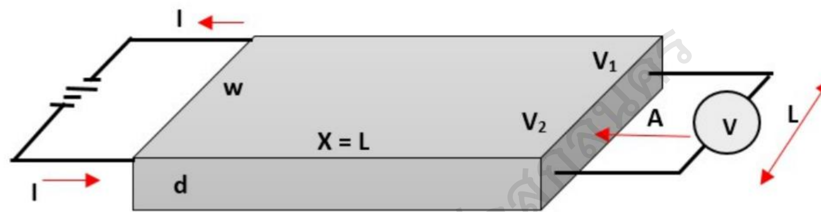

Figure 6 the measurement of electrical resistivity while a current flows through a conductor with a cross section constant.

The current density (J) in the conductor rods as $\frac{I}{A}$ and current flows as $\frac{V_2 - V_1}{L}$ and

$$J = \frac{I}{A} = \frac{\sigma(V_2 - V_1)}{L} \tag{15}$$

According to Ohm's Law, the conductor equation can be expressed as :

$$\sigma = \frac{J}{E} = \frac{\frac{I}{A}}{\frac{(V_2 - V_1)}{L}} \tag{16}$$

มหาวิทยาลัยราชภัฏสกลนคร

With , $(V_2 - V_1) = IV$ write equation (16) as follows :

$$\sigma = \frac{\frac{I}{A}}{\frac{IR}{L}} \tag{17}$$

$$\sigma = \frac{L}{RA} \tag{18}$$

The electrical resistance of the conductor rod length L in figure. 6 is :

$$\sigma = \frac{L}{\sigma A} = \frac{\rho L}{A} \tag{19}$$

When boosting the cross-sectional A as wd and $\rho = \frac{1}{\sigma}$ from equation (19) , so that the new equation as :

$$R = \frac{\rho L}{wd} = \frac{L}{wd}\frac{1}{\sigma} \tag{20}$$

Then, R is electrical resistance (Ω), L is length (m), w is width (m), d is thickness (m). The electrical resistance depends on the nature of the material and electrical resistivity of the same material to the same value.

2. Mobility of carriers

The mobility has ratio of drift velocity with electric field , E ;

$$\mu = \frac{v_{drift}}{E} \tag{21}$$

The mobility electron replace as μ_e and the mobility hole replace as μ_h ,The flow electron in electrical conductivity can be obtained from equation (22)

$$\sigma_e = n_e e \mu_e \tag{22}$$

then n_e is free electrons density.

มหาวิทยาลัยราชภัฏสกลนคร

In the case of semiconductor, wthe electron and hole conductive, the electrical conductivity, written as :

$$\sigma = n_e e \mu_e + n_h e \mu_h \quad (23)$$

then n_h is volume mobility hole.

3. Carrier concentration

The equilibrium, the carrier concentration in intrinsic semiconductor at temperature constant.

The multiplied between density of free electrons and hole as follows:

$$n_o p_o = n_i^2 \quad (24)$$

n_i is the carrier concentration in intrinsic semiconductor.

The carrier density extrinsic semiconductor will majority carriers and the carrier density has less be minority carriers. The density of electrons in the semiconductor n-type (n) are represented by n_n and the density of holes in the semiconductor n-type (n) are represented by p_n. Similarly, the density of hole in the semiconductor p-type (p) are represented by p_p and The density of electrons in the semiconductor p-type (p) are represented by n_p.

The fact that, the crystal structure has to be neutral charge. Therefore, the sum of the charge density in unit volume is equal to zero. For semiconductor impurity is fully charged in two types i.e. Ion static and the charge carrier mobility ions are not mobile i.e. atoms of dopant atoms donor and acceptor (among the elements 3A or 5A).

Since semiconductors have a neutral charge, therefore, the sum of the density of negative charge must be equal. The sum of the positive charge density of the equation.

มหาวิทยาลัยราชภัฏสกลนคร

$$N_a + n = N_d + p \tag{25}$$

N_a is the density of donor, N_d is the density of acceptor, n is the number of electrons, p is the number of hold.

For semiconductor n-type impurity. since there are no acceptor ions the negatively charged. So that N_a is zero and the number of electrons over holes ($n \rangle\rangle p$). So the equation (25) may be rewritten as follows.

$$n_n \cong N_d \tag{26}$$

Equation (26) seen that density of electrons in the n-type semiconductor impurity (n), may be approximately equal to the density of atoms donor doped into. The density of holes in the semiconductor n-type impurity.

$$p_n = \frac{n_i^2}{n_n} \cong \frac{n_i^2}{N_d} \tag{27}$$

For semiconductor p-type impurity (p), The density of holes in a semiconductor. May be approximately equal to the density of atoms acceptor doped into.

$$p_p \cong N_a \tag{28}$$

and density of electron about from equation ;

$$n_p = \frac{n_i^2}{p_p} \cong \frac{n_i^2}{N_a} \tag{29}$$

4. The carrier mobility and carrier density by measuring the Hall (Hall effect measurement)

In 1974, Hall found that if the magnetic field perpendicular to the direction of current flow in conductors, this will cause an electromagnetic field

มหาวิทยาลัยราชภัฏสกลนคร

that is perpendicular to the direction of flow and the direction of the magnetic field inside the conductor. The result of the Lorentz force (Lorentz force) the direction of the light carrier diverted. Make piles on either side of the rod until the conductor electric field up.

The measurement of carrier density and mobility of carriers (Ben G. Streetman, 1995, p.67) can be done using the Hall effect, as shown in Figure 7 based on a semiconductor with a p-type conductivity type. The magnetic field perpendicular to the direction of the hole by the force of the first hole is equal to the sum of the magnetic field and electric field equation.

$$\vec{F} = q(\vec{E} + v\ x\ \vec{B}) \tag{30}$$

Force in the y-axis is

$$F_y = q(E_y - v_x\ B_z) \tag{31}$$

When entering the electric field in the E_x a current flowing in the x-axis and a magnetic field in the B_z Figure 7 is the Lorentz force is equal qv_xB_z in the y-axis. Ran down together beneath an electric field. Acts on the hold and make hold run down together beneath an electric field in +y axis. When the balance will not be gas flowing along the y-axis is the force due to the electric field y equals Lorentz force qv_xB_z in equation

$$qE_y = qv_xB_z \tag{32}$$

It has equation

$$E_y = v_xB_z \tag{33}$$

where $+q$ and p_0 for Holstein is the electric field in the y-axis

$$E_y = \frac{J_x}{qp_0}B_z = R_HJ_x, R_H \equiv \frac{1}{qp_0} \tag{34}$$

where J_x is the current density, R_H is the Hall coefficient.

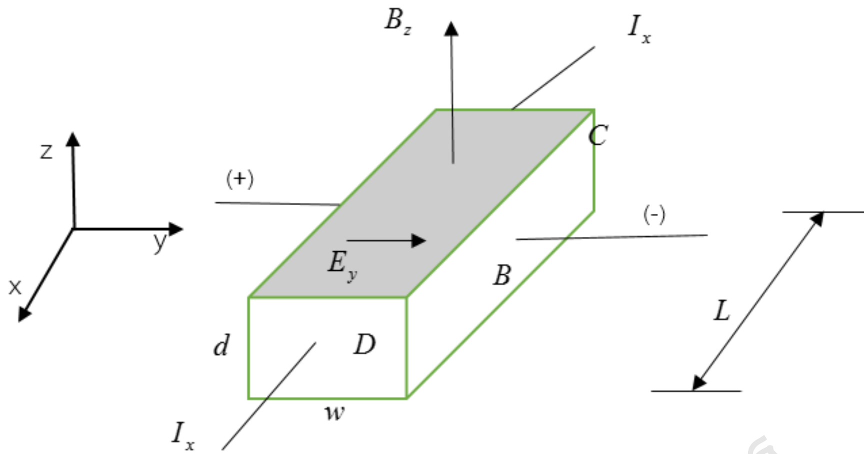

Figure 7 The measurement density of carrier by Hall effect.

Hall field is proportional to the product of current density and magnetic flux density. When the currents and magnetic fields into a measurable voltage Hall (Hall Voltage) and can calculate the density of hold (p_0) in the equation (35)

$$p_0 = \frac{1}{qR_H} = \frac{J_x B_z}{qE_y} = \frac{\left(\frac{I_x B_z}{wd}\right)}{q\left(\frac{V_{AB}}{w}\right)} = \frac{I_x B_z}{qdv_{AB}} \tag{35}$$

Then, the measuring the resistance (R) to calculate electrical resistivity (ρ) as equation :

$$\rho(\Omega cm) = \frac{Rwd}{L} = \frac{\frac{v_{CD}}{I_x}}{\frac{L}{wd}} \tag{36}$$

The thermal conductivity values.

มหาวิทยาลัยราชภัฏสกลนคร

$$\sigma = \frac{1}{\rho} = q\mu_p p_0 \tag{37}$$

Then, μ_0 is mobility carrier of hole.

The mobility carrier of hole is the ratio of the Hall coefficient and thermal conductivity. as equation :

$$\mu_p = \frac{\sigma}{qp_0} = \frac{\frac{1}{\rho}}{q\left(\frac{1}{qR_H}\right)} = \frac{R_H}{\rho} \tag{38}$$

AgSbTe COMPOUNDS

The ternary chalcogenides $AgSbTe_2$ belong to the family of semiconductors with a disordered NaCl cubic structure; $AgSbTe_2$ is not only a good thermoelectric but is the end compound of several high-temperature, high-performance thermoelectric. The electrical conductivity measurements show a metallic behavior of $AgSbTe_2$, whereas the diffuse reflectance suggests an apparent band gap (0.35 eV). $AgSbX_2$ (X = Se,Te) compounds are related to zinc-blende structures. Rock salt $AgSbTe_2$ was synthesized in 1957 (S. Berri et al, 2012, pp. 3320-3327).

The Ag compounds show an importance in thermoelectric, optical phase change, and frequency conversion applications. In comparison with the classical GeSbTe phase change memory alloy, AgVInSbTe is reported to have better erasability and cyclability in memory switching. It was found that the compounds under study have undergone a transition phase from B1 to B2 between 17 and 26 GPa for $AgSbTe_2$. A transition under temperature was observed from solids to liquids at T = 849 K for $AgSbTe_2$. In recent years the perovskite ABX_3 type compounds have numerous technological applications due to their wide range of attractive properties, ferroelectricity, piezoelectricity,

semiconductivity, catalytic activity, thermoelectricity, superconductivity and metal–insulator transition. Example ternary oxides of rare earth (Eu, Gd and Tb) CoO_3 are important materials because of their electrical, magnetic and catalytic properties.

The perovskite type oxides in this series find extensive application in materials science and technology, some of the perovskite (Eu, Gd and Tb) CoO_3 compounds are used as electrode materials for magnetohydrodynamic (MHD) generators and for fuel cells. In general, $AgSbTe_2$ compounds crystallize in the cubic space group Fm3m(#225) .

The Ag atom are positioned at the (0 0 0) position, the Sb atom at the (0.5 0.5 0.5) position and Te atom at the (0.25 0.25 0.25) position. On the other hand the compounds ABX_3 crystallize in the cubic space group Pm3m(#221). The crystal structure of these compounds is shown in Figure 8.

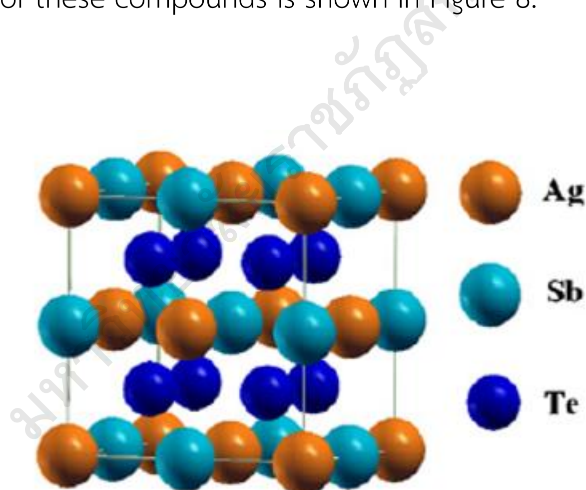

Figure 8 Crystal structure of $AgSbTe_2$ compounds (S. Berri, 2012).

1. Structural properties

The calculated total energy of $AgSbTe_2$ using FP-LAPW and PPPW methods, the plots of calculated total energies versus reduced volume for these compounds are given in Figure 9 The total energies versus changed volumes are fitted to Murnaghan's equation of state in order to determine the ground state

properties, such as equilibrium lattice constant a, bulk modulus B and its pressure derivative B'.

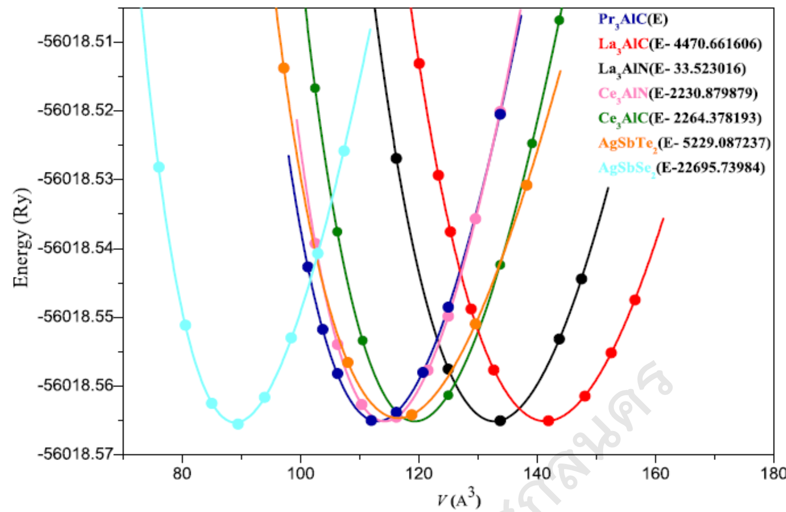

Figure 9 Calculated total energies as a function of volume of $AgSbTe_2$, $AgSbSe_2$, Pr_3AlC, Ce_3AlC, Ce_3AlN, La_3AlC and La_3AlN compounds (S. Berri, 2012).

2. Electronic structure

1. Band structure

The band structures for those compounds have been calculated at the theoretical equilibrium lattice constant by using FP-LAPW and PP-PW methods along high-symmetry directions of the first Brillouin zone are plotted in Figure 10 Note that, there is no difference in the band structure plot for the two methods.

The conduction band minimum (CBM) is found to be mixed with the valence band maximum (VBM) along the (XX) direction for $AgSbTe_2$ from the two methods. The experimental value of the band gap for $AgSbTe_2$ is 0.71 eV, obtained by using direct gap-optical measurements. While Abdel-ghany et al. found a band gap of 1.65 eV by using indirect gapoptical measurements. One reason of this discrepancy is that in our calculations, we haveassumed the crystal to be at T = 0 K and thus do not include contributions from lattice vibrations that are present at room temperature measurements.

มหาวิทยาลัยราชภัฏสกลนคร

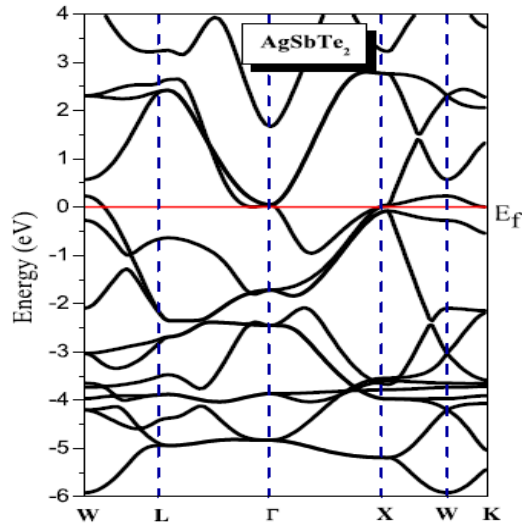

Figure 10 Band structure for high-symmetry directions in the Brillouin zone of $AgSbTe_2$ compounds (S. Berri, 2012).

มหาวิทยาลัยราชภัฏสกลนคร

2. Total and partial density of states.

To further elucidate the nature of the electronic band structure, we have calculated the total and the partial densities of states (DOS) of these compounds. These are displayed in Figure 11. It can be noted that the DOS of $AgSbTe_2$ can be mainly divided into three parts : the first part extending from -10 eV to -8 eV the contribution of Sb-s, the second part from - 8 eV to 0 eV is of the combination of Ag (de_g and dt_{2g}) and Te-p and the third part extended from 0 eV to 4 eV, this structure originates from Sb-p states.

3. Charge density

In order to understand the nature of chemical bonding, we display, in Figure 12, the contours of charge densities in the (1 1 0) plane for those compounds by using the FP-LAPW method. In the case of $AgSbTe_2$ compounds, the overall shape of the charge distributions suggests a partially ionic bonding in both Te–(Ag, Sb) bonds. We can conclude that the bonding in $AgSbTe_2$ is a purely ionic character.

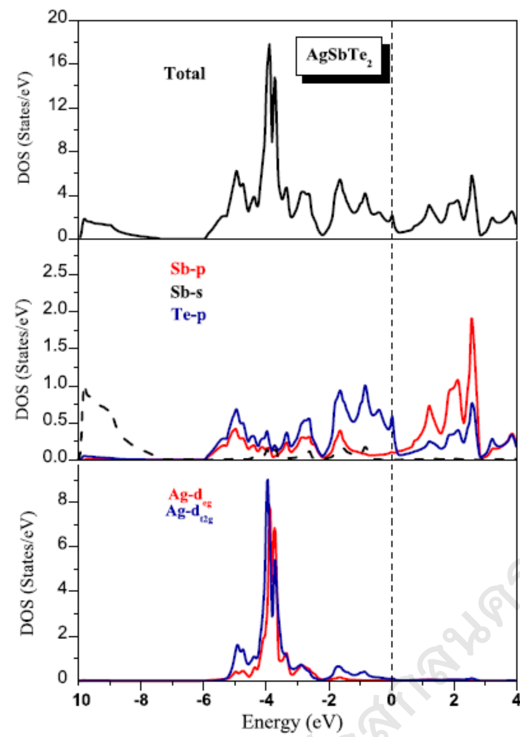

Figure 11 Total and partial DOS of $AgSbTe_2$ compounds (S. Berri, 2012).

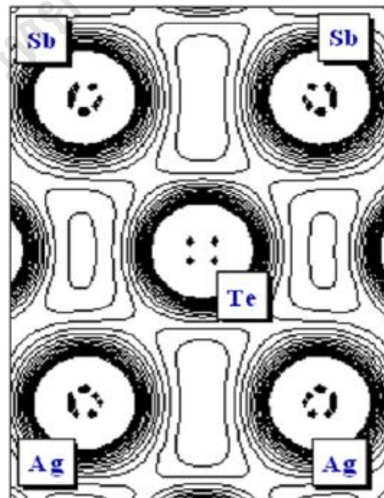

Figure 12 Charge density distribution in the plan (1 1 0) of $AgSbTe_2$ compounds (S. Berri, 2012).

มหาวิทยาลัยราชภัฏสกลนคร

THIN FILM CHARACTERIZATION

1. X-ray diffraction method

The XRD was performed by using an X-ray diffractometer equipped with CuK_α radiation, λ = 0.15406 nm (Model PW 1830, Philips) at 30 kV and 30 mA. The scanning mode was θ-2θ with scanning range and rate of $10^\circ \le 2\theta \le 70^\circ$ and 0.02° /sec, respectively.

The X-ray diffraction (XRD) method is a method used to determine the crystal structure, lattice constant and grain size of the thin film. In the XRD method, the X-rays from the generator are sent towards the films and scattered to the detector, with each atom in the crystal lattice acting as a source of scattering. By considering how the crystal lattice reflects from parallel reflecting planes, as shown in Figure 13, the maximum intensity of the reflected beam of X-ray can be obtained when the path difference between two reflected waves of two different planes is an integral multiple of wavelengths.

มหาวิทยาลัยราชภัฏกำแพงเพชร

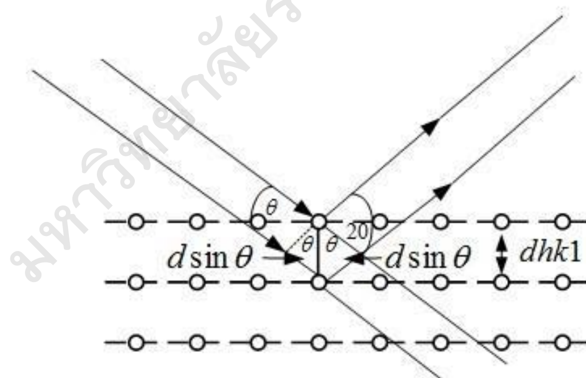

Figure 13 The parallel reflecting planes of crystal lattice, path difference of two reflected wave (red lines).

The condition can be explained using Bragg’s law and is given by the relation,

$$2d_{hkl}\sin\theta = n\lambda \tag{39}$$

where d_{hkl} is inter planar spacing of the reflection planes, λ is the wavelength of the CuK$_\alpha$ radiation, θ is the Bragg's angle and n is an order of diffraction. The lattice constant of the cubic zinc blend structure can be calculated by the following relation.

$$\frac{1}{d_{hkl}} = \sqrt{\frac{h^2 + k^2 + l^2}{a^2}} \tag{40}$$

where d_{hkl} is the inter planar spacing of the reflection planes, h, k and l are Miller'sindices and a is the lattice constant.

The crystallite size (D) can be estimated from the full width at half maximum (FWHM) of the XRD peak using the Debye-Scherer relation,

$$D = \frac{k\lambda}{B_s \cos\theta} \tag{41}$$

where k = 0.9 is a constant, λ is the wavelength of the CuK$_\alpha$ radiation, B_s is the full width at half maximum contribution from the grain size effect and θ is the angular position of the peak. The corrected peak width (B_s) of FWHM of the structure can be calculated from the formula $B_s^2 = B_o^2 - B_i^2$ where B_o is the observed data and B_i is the FWHM of the instrument

2. Scanning Electron Microscopy

The Scanning Electron Microscopy (SEM) was used to observe microstructures of the samples. The SEM observations were performed on a Hitachi High Technologies, S-2600H. The schematic diagram of the SEM equipment is shown in Figure 14.

มหาวิทยาลัยราชภัฏสกลนคร

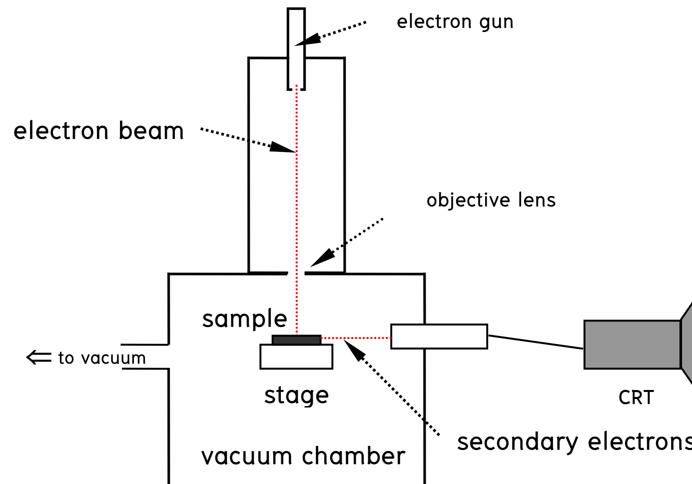

Figure 14 Diagram of the scanning electron microscope technique

มหาวิทยาลัยราชภัฏสกลนคร

3. Atomic Force Microscope

Atomic force microscopy (AFM) or scanning force microscopy (SFM) is a very-high-resolution type of scanning probe microscopy (SPM), with demonstrated resolution in the order of fractions of a nanometer, more than 1000 times better than the optical diffraction limit. The information is gathered by "feeling" or "touching" the surface with a mechanical probe. Piezoelectric elements that facilitate tiny but accurate and precise movements on (electronic) command enable precise scanning.

4. Elemental Composition

Energy Dispersive X-ray spectroscopy (EDX) was used to analyze the elemental compounds and distribution of thin film. In this method, the specimen is excited by high-energy electrons and the emitted X-ray energies correspond to the characteristics of the elements within the specimen. The emitted X-rays can be used to identify elements and the relative composition can be estimated. The elemental composition of thin films can be obtained using an EDX detector which is attached to a TEM system (Tecnai G^2).

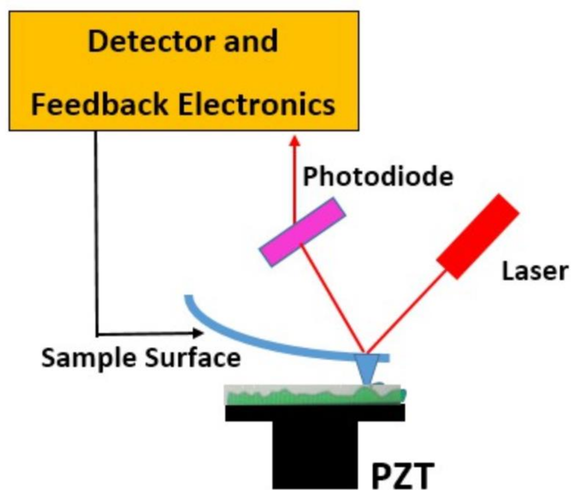

Figure 15 Diagram of the scanning electron microscope technique. Atomic force microscopy.

มหาวิทยาลัยราชภัฏสกลนคร